Technique for the Prediction of Airfoil Flutter Characteristics in Separated Flow

Jiunn-Chi Wu*
National Central University, Chong-Li, Taiwan
K. R. V. Kaza†
NASA Lewis Research Center, Cleveland, Ohio
and
L. N. Sankar‡
Georgia Institute of Technology, Atlanta, Georgia

A solution procedure is described for determining the two-dimensional, one- or two-degree-of-freedom flutter characteristics of arbitrary airfoils at large angles of attack. The same procedure is used to predict stall flutter. This procedure requires a simultaneous integration in time of the solid and fluid equations of motion. The fluid equations of motion are the unsteady compressible Navier-Stokes equations, solved in a body-fitted moving coordinate system using an approximate factorization scheme. The solid equations of motion are integrated in time using an Euler implicit scheme. Flutter is said to occur if small disturbances imposed on the airfoil attitude lead to divergent oscillatory motions at subsequent times. Results for a number of special cases are presented to demonstrate the suitability of this scheme to predict flutter at large mean angles of attack. Some stall flutter applications are also presented.

Nomenclature

a = speed of sound
a_h = offset of elastic axis in the structural model
b = semichord length
c = airfoil chord length
C_L = lift coefficient
C_M = moment coefficient
C_P = pressure coefficient, $2(p - p_\infty)/\rho_\infty V_\infty^2$
e = total energy per unit volume
g_h, g_α = structural damping coefficients in the structural model
h = airfoil vertical displacement
I = identity matrix
I_α = moment of inertia
J = Jacobian of transformation
k_b = reduced frequency based on semichord length, $\omega_f b/V_\infty$
K_h, K_α = spring constants in the structural model
L = lift
m = airfoil mass per unit span
M = moment
M_∞ = freestream Mach number
p = pressure
Re = Reynolds number, $\rho_\infty V_\infty c/\mu_\infty$
t = nondimensional physical time
u, v = Cartesian velocity components
V^* = dimensionless speed, $v_\infty/b\omega_\alpha$
x, y = physical Cartesian coordinates
x_α = static unbalance in the structural model, sa/mb
α = angle of attack
ϵ_E, ϵ_I = coefficients of artificial dissipation
μ = airfoil-to-air-mass ratio, $m/\pi\rho_\infty b^2$
ξ, η = transformed coordinates
ρ = density
τ = transformed time
ω_f = frequency of oscillation
ω_h = natural frequency in plunging
ω_α = natural frequency in pitching

Received March 23, 1987; presented as Paper 87-0910 at the AIAA Dynamics Specialists Conference, Monterey, CA, April 9-10, 1987; revision received Aug. 15, 1988.

*Associate Professor, Department of Mechanical Engineering.
†Senior Research Engineer. Associate Fellow AIAA.
‡Associate Professor, School of Aerospace Engineering. Member AIAA.

Introduction

THE operating conditions of modern propfan and turbomachinery configurations often include situations where highly separated flows may occur. Under certain conditions, unsteady lift and pitching moments may develop that lead to an input of energy from the airstream onto the blade structure and thus to a rapid growth in the structural oscillations. This phemenon is called stall flutter and must be predicted accurately enough for safe and efficient aeroelastic design of these structures. Existing analytical tools for the prediction of stall flutter treat this problem as a structure/fluid interaction problem. Since the unsteady aerodynamics associated with this phenomenon is complex, researchers have in the past relied on experimental data for airfoil static and dynamic stall characteristics. These data are usually synthesized into a series of analytical expressions for different parts of the dynamic stall loop and used in a flutter analysis. Currently, a number of empirical models are available for the static and dynamic stall load characteristics of airfoils for a wide variety of flow conditions.[1,2] A comparative study of a variety of analytical models for the prediction of the dynamic stall phenomenon has recently been carried out by Reddy and Kaza.[3]

There are two ways in which the existing technology can be improved. In the first approach, reliable and accurate Navier-Stokes solvers can be used to generate the static and dynamic stall characteristics of arbitrarily shaped airfoils for a wide range of flow conditions. The aerodynamic loads generated by these solvers can then be synthesized in the same way that the experimental data would be synthesized. This reduces the reliance of the stall flutter analysis on the availability of a large body of experimental data.

In the second approach, the structural/fluid dynamics equations can be simultaneously integrated in time. The aerodynamic loads determined from the integration of the unsteady, compressible Navier-Stokes equations drive the structural dynamics equations. The resulting structural deformations alter the aerodynamic loads. Under certain conditions, the coupling between the aerodynamic loads and the structural motion is such that small disturbances imposed on the airfoil angle of attack grow rapidly, in a divergent oscillatory fashion, and flutter occurs.

The idea of simultaneously integrating the solid and fluid equations of motion is not new in itself, but has in the past been applied primarily with simpler aerodynamic analyses and for small angle-of-attack conditions. Ballhaus and Goorjian[4] developed a solution procedure for solving two-dimensional unsteady potential flows subject to the low-frequency, small-disturbance assumptions. They used this procedure to study the single-degree-of-freedom (DOF) flutter problem through a simultaneous integration of the solid and fluid equations of motion. A number of other researchers have since then applied the transonic small-disturbance (TSD) theory to predict the flutter characteristics of conventional and supercritical airfoils.[5-8] To a smaller extent, potential flow solvers of the compressible unsteady full potential equation are also being applied to two-dimensional aeroelastic calculations.[9,10] Some of these approaches account for weak viscous interactions through a solution of the two-dimensional integral boundary-layer equation.

In three dimensions also, computer codes that solve the unsteady transonic small-disturbance equation or the unsteady full potential equation have been the primary tools for aeroelastic analysis. Some typical applications of the transonic potential flow theory to three-dimensional aeroelastic problems may be found in Refs. 11–14. An excellent survey of computational methods for predicting transonic flutter phenomena in the attached and mildly separated flow regime may be found in Ref. 15.

While the above-mentioned approaches are adequate for a number of applications, the potential flow theory becomes invalid in some situations. The potential flow assumption breaks down for thick airfoils at high transonic freestream Mach numbers (0.9 or above) and at high angles of attack. The shock location and the shock strength predicted by the potential flow theory are suspect whenever the local Mach number upstream of the shock exceeds 1.2. Furthermore, potential flow theory can give multiple steady-state solutions at a given flow condition if the freestream Mach number is sufficiently high. This nonuniqueness problem makes potential flow theory unsuitable above low transonic Mach numbers (0.85 or above) for thick airfoils.

The second drawback of potential flow approximations is their inability to account for large viscous effects. Stall flutter and transonic aileron buzz are just two examples of problems requiring a detailed modeling of viscous effects. Whenever significant flow separation exists, the use of inviscid solution techniques based on potential flow on Euler equations becomes invalid.

Thus, a need exists in the field of computational aeroelasticity for flow solvers in two and three dimensions that can account for the rotational effects at high freestream Mach numbers and separation or stall. Except for a few studies where this has been addressed (e.g., Ref. 16 where the aileron buzz problem was addressed by Steger and Bailey), the authors are not aware of flow solvers that can meet these needs. It is the long-term objective of the present research to develop a reliable aeroelastic analysis capability, particularly within the context of propfan and turbomachinery stall futter. As a first step toward this goal, a solution technique capable of predicting airfoil flutter at large mean angles of attack has been developed here. Some promising results for the stall flutter problem have also been obtained.

In the present work, the full unsteady compressible Navier-Stokes equations are solved in a body-fitted moving coordinate system. The flow solver described in Ref. 17 has been modified for this purpose. This solver provides the aerodynamic loads input to a two-DOF structural dynamics model. The structural dynamics equations, which are coupled second-order ordinary differential equations in time, are solved by a one-step, first-order-accurate implicit time-marching procedure.

Since there is a need to carefully validate any aerodynamics model prior to its application to flutter calculations, a number of code validation studies are first presented, including some cases where deep dynamic stall occurs. Following the code validation, the present technique is applied to one- and two-DOF flutter problems. Finally, two stall flutter applications are presented.

Mathematical and Numerical Formulation

In this section, the numerical procedure used to compute the unsteady viscous flow over arbitrary airfoil geometries is briefly described.

All the calculations were performed in a transformed coordinate system (ξ,η,τ), which is linked to the physical plane (x,y,t) according to the following one-to-one relationship:

$$\xi = \xi(x,y,t), \quad \eta = \eta(x,y,t), \quad \tau = t \tag{1}$$

The Jacobian of transformation J is given by

$$J = \xi_x \eta_y - \xi_y \eta_x \tag{2}$$

and the metrics of transformation are given by

$$\xi_x = Jy_\eta, \quad \xi_y = -Jx_\eta, \quad \eta_x = -Jy_\xi, \quad \eta_y = Jx_\xi \tag{3}$$

Two types of body-fitted grids were used in the present study. The first type of grid is an algebraic C-type grid generated using a sheared parabolic grid construction, followed by an algebraic clustering of the C-lines in the vicinity of the airfoil. The second type of grid is also a C-type grid, generated using the GRAPE grid generation program.[18]

Once a grid has been constructed, the metrics of the transformation may be evaluated numerically. Standard central differences were used to compute quantities such as x_ξ, x_η, etc., which in return were used to compute quantities such as ξ_x, ξ_y, etc. At the solid surface and the inflow/outflow boundaries, three-point one-sided differences were used to compute the metrics.

In the (ξ,η,τ) coordinate system, the two-dimensional, unsteady Navier-Stokes equations may be written as

$$\boldsymbol{q}_\tau + \boldsymbol{F}_\xi + \boldsymbol{G}_\eta = (1/Re)(\boldsymbol{R}_\xi + \boldsymbol{S}_\eta) \tag{4}$$

where

$$\boldsymbol{q} = J^{-1}\{\rho, \rho u, \rho v, e\} \tag{5}$$

The quantities $\boldsymbol{F}$, $\boldsymbol{G}$, $\boldsymbol{R}$, and $\boldsymbol{S}$ are given by

$$\begin{aligned} \boldsymbol{F} &= (\xi_x F + \xi_y G + \xi_t q)/J \\ \boldsymbol{G} &= (\eta_x F + \eta_y G + \eta_t q)/J \\ \boldsymbol{R} &= (\xi_x R + \xi_y S)/J \\ \boldsymbol{S} &= (\eta_x R + \eta_y S)/J \end{aligned} \tag{6}$$

$$F = \begin{bmatrix} \rho u \\ \rho u^2 + p \\ \rho uv \\ u(e+p) \end{bmatrix} \quad G = \begin{bmatrix} \rho v \\ \rho uv \\ \rho v^2 + p \\ v(e+p) \end{bmatrix} \quad R = \begin{bmatrix} 0 \\ \tau_{xx} \\ \tau_{xy} \\ R_4 \end{bmatrix} \quad S = \begin{bmatrix} 0 \\ \tau_{xy} \\ \tau_{yy} \\ S_4 \end{bmatrix} \tag{7}$$

The quantities R_4 and S_4 represent the dissipation of energy due to work done by the viscous stresses and heat conduction along the x and y directions, respectively. The viscous stresses τ_{xx}, τ_{xy}, and τ_{yy} were related to the velocity gradients through Stokes' hypothesis. Note that in the present work all the calculations are done with respect to an inertial observer and not in a rotating frame. Thus, explicit centrifugal and Coriolis terms do not occur in Eq. (4). These body forces, of course, are accounted for by the time and spatial derivatives of the grid velocity x_τ and y_τ in Eq. (6).

Since the governing equations are coupled to each other and are highly nonlinear, a stable, efficient solution procedure is required for solving them. In the present work, the Beam-Warming algorithm[19] as implemented by Steger[20] was used with some modifications. The viscous terms were explicitly evaluated using information available at earlier steps. Explicit evaluation of the viscous terms greatly reduces the number of operations needed to solve the governing equations. Since the mathematical and numerical formulation of the Beam-Warming algorithm are well known, only a brief description of the solution scheme is given here.

The governing equations are written as a computational node (i,j) in the following finite-difference form:

$$\delta_\tau q^{n+1} + \delta_\xi E^{n+1} + \delta_\xi G^{n+1} = \delta_\xi R^n + \delta_\eta S^n - \epsilon_E D^n \tag{8}$$

where, for example, the term $\delta_\xi F^{n+1}$ is the standard two-point central-difference formula given by $(F_{i+1} - F_{i-1})^{n+1}/2$. The quantity D is an artificial dissipation term, added to remove high-frequency errors in the solution at every time step and to avoid odd-even decoupling of the numerical solutions. For a detailed description of the artificial dissipation term formulation as employed in this work, the reader is referred to Ref. 17.

The highly nonlinear terms F and G at the time level $(n+1)$ were expanded by a Taylor series about a previous time level n as

$$F^{n+1} = F^n + [DF/Dq]^n(q^{n+1} - q^n)$$

$$G^{n+1} = G^n + [DG/Dq]^n(q^{n+1} - q^n) \tag{9}$$

where the quantities $[DF/Dq]$ and $[DG/Dq]$ are 4×4 matrices that are the Jacobians of the flux vectors F and G with respect to q.

In order to allow large values of the explicit dissipation coefficient ϵ_E to be used without instability and to allow the viscous terms to be treated explicitly, the following implicit dissipation terms were added to the left side of Eq. (8):

$$-\epsilon_I J^{-1}(\delta_{\xi\xi} + \delta_{\eta\eta})J(q^{n+1} - q^n) \tag{10}$$

The coefficient ϵ_I was taken to be three times the explicit dissipation coefficient ϵ_E. A range of ϵ_E values between 3 and 5 were used in the calculations reported here.

Equation (8) may be written after the addition of the artificial implicit dissipation terms given by Eq. (10), in the following operator form:

$$[I + \Delta\tau(\delta_\xi\{DF/Dq\} + \delta_\xi\{DF/Dq\}) - \Delta\tau\epsilon_I J^{-1}(\delta_{\xi\xi} + \delta_{\eta\eta})J]$$

$$\times (q^{n+1} - q^n) = R^n \tag{11}$$

where

$$R^n = -\Delta\tau(\delta_\xi F + \delta_\eta G)^n + \Delta\tau(\delta_\xi R + \delta_\eta S)^n - \Delta\tau\epsilon_E D^n \tag{12}$$

The left-hand-side operator of Eq. (11) was approximately factored into two smaller operators, leading to the following final form:

$$[I + \Delta\tau(\delta_\xi\{DF/Dq\} - \epsilon_I J^{-1}\delta_{\xi\xi}J)][I + \Delta\tau(\delta_\xi\{DF/Dq\}$$

$$- \epsilon_I J^{-1}\delta_{\eta\eta}J)](q^{n+1} - q^n) = R^n \tag{13}$$

Equation (13) may be solved through the inversion of two block tridiagonal matrix equations, one corresponding to the ξ direction and the other to the η direction. In order to keep the flow solver simple, the boundary conditions on all the boundaries were explicitly updated after the interior points had been updated using Eq. (13).

The boundary conditons employed at all the computational boundaries were as follows. At the solid surface, the no-slip boundary conditions were enforced by setting the velocity of the fluid to that of the solid at every time step. At the solid surface, the normal derivatives of temperature and pressure were also set to zero. The use of the C-grid system introduces a cut between the airfoil trailing edge and the downstream boundary. Along this cut, the flow properties were averaged from above and below. The body-fitted grids employed in this work were such that the far-field boundaries were at least six chord lengths away. Therefore, in the calculations described here, the flow properties at these boundaries were assumed to be undisturbed.

In turbulent flows, the turbulent shear stresses were modeled using an eddy viscosity concept. A two-layer eddy viscosity model developed by Baldwin and Lomax was used in these studies.[21]

The Navier-Stokes solver described here may also be used to model inviscid rotational flows. This requires that the viscous terms in the Navier-Stokes equations be suppressed and that the zero tangential velocity boundary condition at the solid surface be replaced by a nonzero value, obtained by extrapolating the tangential component of the fluid velocity from the interior.

Structural Dynamic Model

The structural dynamics model considered is a two-DOF system, free to rotate in the x-y plane and free to translate up or down. Resisting elastic forces are developed that are proportional to the airfoil torsional and translational displacement; the motion of the airfoil is further hampered by structural damping forces that are proportional to its angular or translational velocity. In Fig. 1, a sketch of the two-DOF system is shown. Note that the pitching axis may be offset from the center of mass of the airfoil, leading to a coupling between the pitching and plunging degrees of freedom. The equations governing the motion of the two-DOF system are

$$S_\alpha\ddot{h} + I_\alpha\ddot{\alpha} + g_\alpha\dot{\alpha}K_\alpha\alpha = M(t)$$

$$m\ddot{h} + S_\alpha\ddot{\alpha} + g_h\dot{h} + K_h h = -L(t) \tag{14}$$

where h is the airfoil vertical displacement, α the angular displacement (angle of attack), I_α the airfoil moment of inertia (per unit span) about the pitching axis, and m and S_α the mass and static moment per unit span, respectively. The K_α and K_h are the spring constants for the pitching and plunging motion, respectively, and g_α and g_h are the structural damping coefficients for the pitching and plunging motion, respectively. The S_α depends on the offset between the airfoil pitching axis and the airfoil center of gravity.

In the present work, an implicit time marching technique was used to integrate equation set (14). Let n be the time level where

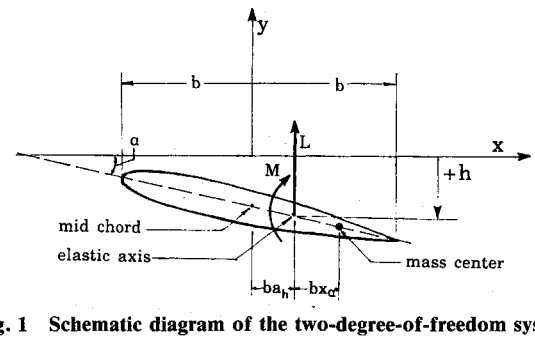

Fig. 1 Schematic diagram of the two-degree-of-freedom system.

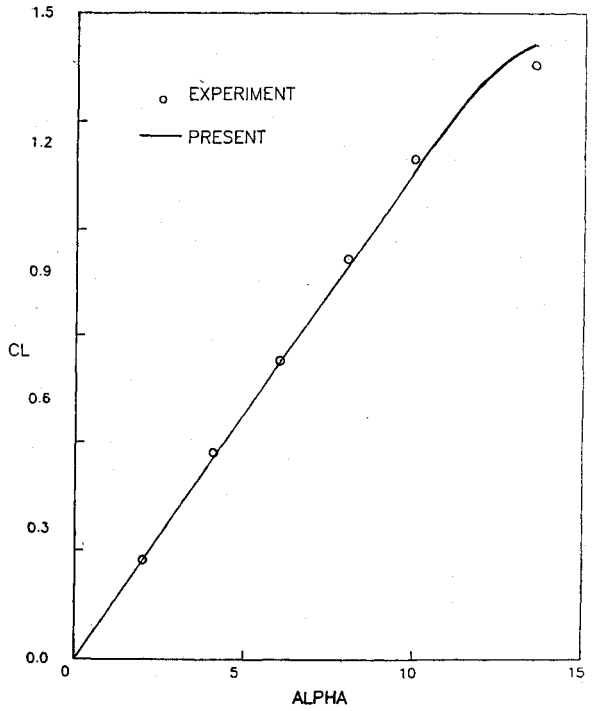

Fig. 2 Comparisons of theory vs experiment for the variation of lift coefficient as a function of angle of attack for the NACA 0012 airfoil ($M_\infty = 0.301$, $Re = 3.9 \times 10^6$).

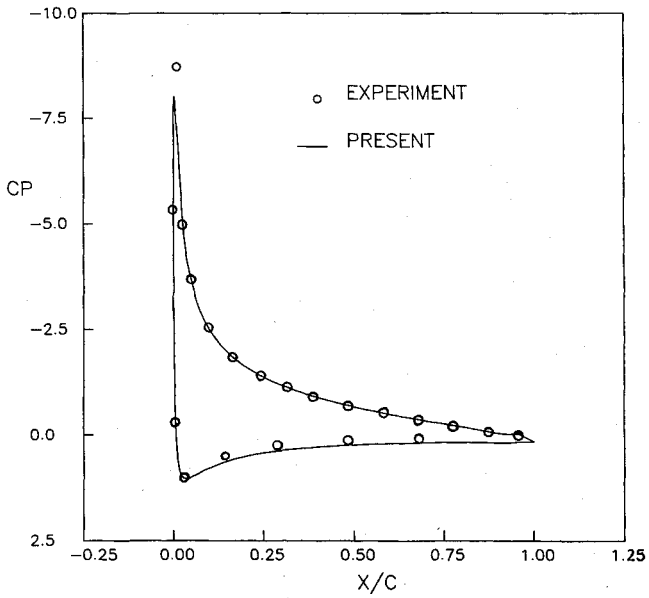

Fig. 3 Comparisons of theory vs experiment for the surface distribution over a NACA 0012 airfoil at 13.5 deg angle of attack ($M_\infty = 0.301$, $Re = 3.9 \times 10^6$).

the solution is known and $n + 1$ is the time level where h and α are sought. Then, the first and second derivatives of h and α were written as

$$\dot{h} = [(h^{n+1} - h^n)/\Delta t]$$

$$\ddot{h} = [h^{n+1} - 2h^n + h^{n-1})/\Delta t^2], \text{ etc.} \qquad (15)$$

Substituting these finite-difference derivatives for h, $\dot{h}$, α, and $\dot{\alpha}$ into equation set (14) leads to a system of simultaneous equations for h^{n+1} and α^{n+1} at each time step.

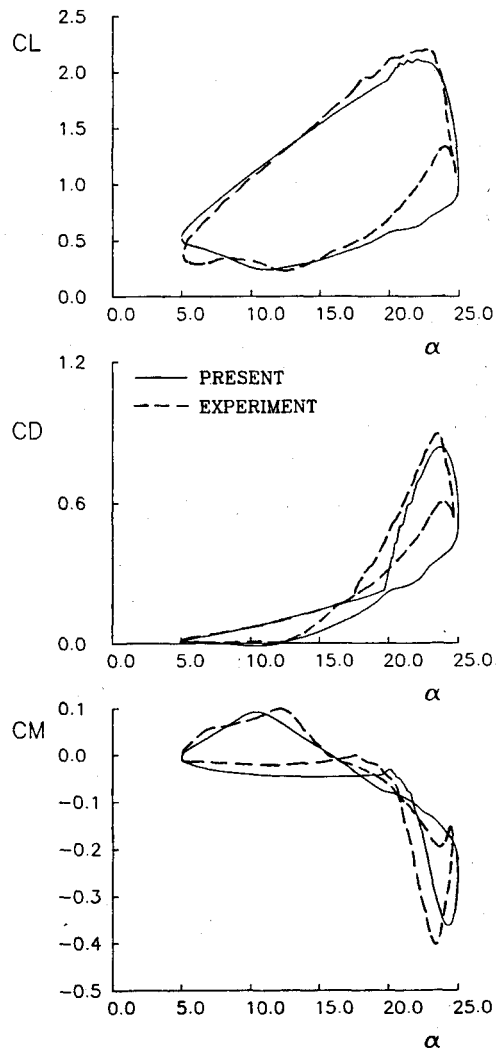

Fig. 4 Comparisons of theory and experiments for the unsteady airloads on a NACA 0012 airfoil experiencing dynamic stall ($M_\infty = 0.283$, $Re = 3.45 \times 10^6$, $k_b = 0.151$).

The flutter calculations described here were done using the following approach. First, the steady-state solution for the flow around the airfoil was obtained using the Navier-Stokes solver for the specified freestream conditions. Once the steady-state solution was obtained, a small-amplitude random perturbations was applied to the airfoil. That is, small nonzero values of $\dot{h}$ and $\dot{\alpha}$ were specified. From that point onward, the fluid equations and the solid equations were simultaneously integrated in time to monitor how $L(t)$, $M(t)$, h, and α varied with time. Flutter was said to occur if these values tended to grow in an oscillatory fashion.

If the starting point of these calculations is near the static stall angle or in the middle of a dynamic stall loop, note that this approach may be used to predict stall flutter. A third DOF, corresponding to an oscillating trailing-edge surface may be readily added to the present solver, since the flow solver and the grid generation techniques employed here can handle arbitrary airfoil shapes and arbitrary time-deforming grids.

Results and Discussions

Code Validation Studies

Prior to the application of this computer code in flutter applications, the flow solver was extensively calibrated for a number of test cases. In this work, only a few of these calibration studies are reported. The interested reader is referred to Ref. 17 for additional code validation studies and application of this solver to supercritical airfoil studies. A 161 × 41 grid was

used in these studies, requiring approximately 0.26 s per time step on a Cray XMP computer. Some calculations were also done on a 253 × 58 grid to assess the effect of grid density on the solution. These grid studies are documented in Ref. 17. The time step was 0.005 based on the chord and speed of sound. Solution for a typical cycle of oscillation required 14,000 time steps. Steady-state solutions required 2000 time steps, when spatially varying time steps were used.

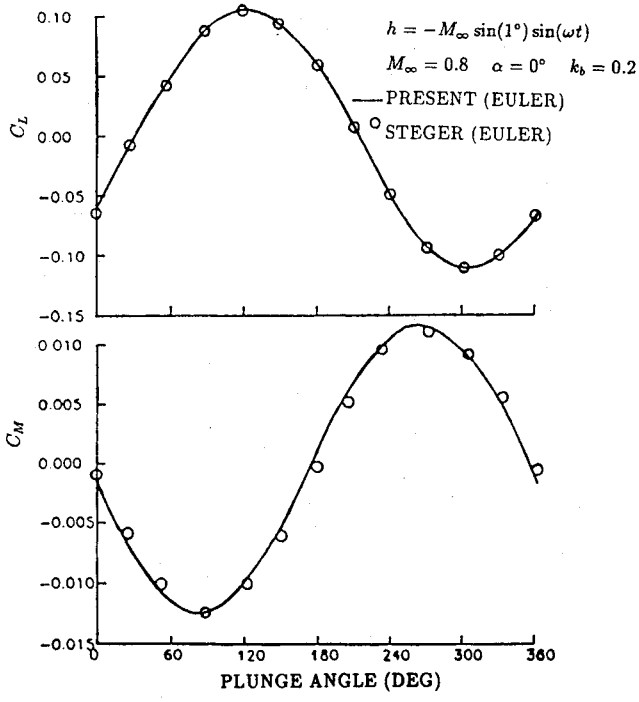

Fig. 5 Variation of lift and pitching moment coefficient for a NACA 64A010 airfoil experiencing sinusoidal plunging motion.

In Fig. 2, the lift vs angle of attack curve is plotted for a NACA 0012 airfoil for angles of attack of 0–15 deg. The freestream Mach number and Reynolds number were 0.3 and 3.9×10^6, respectively. For comparison, experimental data obtained by McAlister et al.[22] are also shown. The present results and the experiments are seen to be in good agreement, up to the stall onset occurring around 14 deg.

In Fig. 3, the surface pressure distribution for the same airfoil at 13.5 deg angle of attack is shown for the flow conditions considered in Fig. 2 and compared with the experiments. Again, a good agreement between the theory and the experiment is observed everywhere except in the immediate vicinity of the airfoil leading edge, where the theory tends to underpredict the suction peak.

In order to illustrate the capability of the Navier-Stokes solver to obtain time-accurate results in highly separated flow, the lift, drag, and moment hysteresis loops are shown and compared with experiments[22] in Fig. 4 for a NACA 0012 airfoil oscillating in pitch. The mean angle of oscillation was 10 deg. The reduced frequency of oscillation, normalized with respect to the half-chord, was 0.151. The freestream Mach number and Reynolds number were 0.283 and 3.45×10^6, respectively. It is seen that the theory correctly predicts the near-linear increase in lift during the upstroke, the dynamic stall causing rapid variations in lift, drag, and moment alike, and the poststall recovery phase of the flow during the downstroke. The fact that the flow solver is able to capture much of the dynamic stall flow features increases the confidence in the capability of this code to handle stall flutter problems.

As a final test of the above solver's ability to handle unsteady transonic flows in a time-accurate manner, the flow over a NACA 64A010 airfoil oscillating sinusoidally in plunge at a freestream Mach number of 0.8 at zero mean angle of attack was considered. The plunging motion produced a maximum apparent angle of attack equal to 1 deg and the reduced frequency based on semichord was 0.2. In Fig. 5, the lift and pitching moment history are plotted as a function of phase and are compared with the Euler calculations performed by Steger.[20] Very good agreement is observed between the two

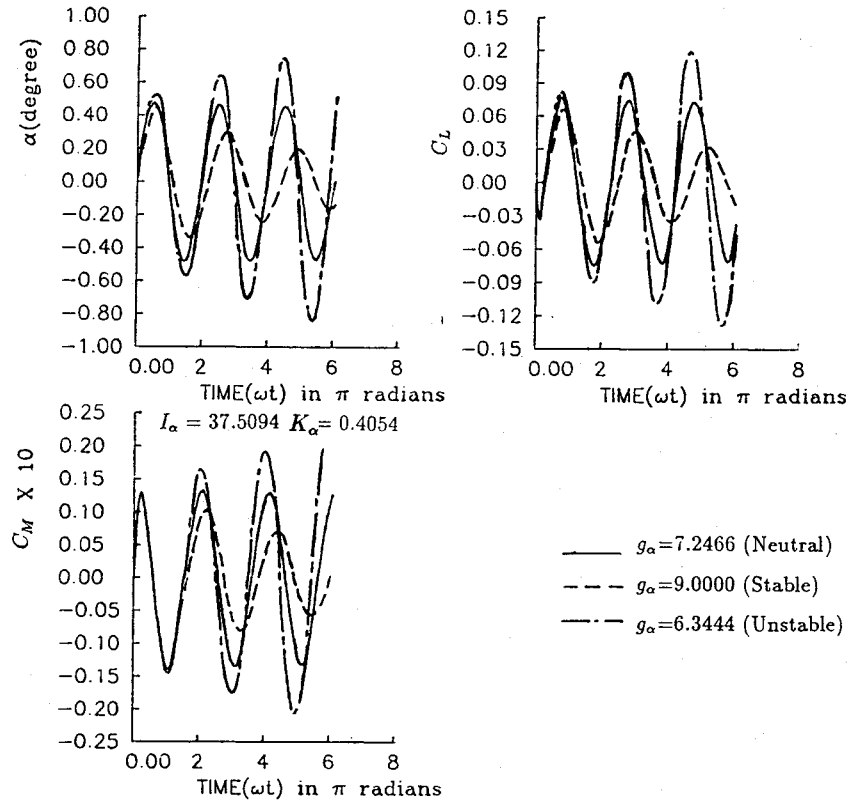

Fig. 6 Response of the solid-fluid system as a function of time (NACA 64A006 airfoil, $M_\infty = 0.90$, single degree of freedom in pitch, inviscid solution).

solvers, despite the fact that the two solvers use different grids and contain different artificial dissipation formulations.

Transonic Flutter

Although the objective of this research is to develop techniques for the prediction of stall flutter, several inviscid one- and two-DOF flutter calculations were first carried out for cases where reliable numerical solutions exist. The transonic flutter calculations were carried out in the following order. First, a steady flow solution was generated for the candidate airfoil, at the prescribed mean angle of attack and Mach number. Next, a series of calculations were carried out for the airfoil undergoing forced sinusoidal pitching or plunging motion, at a user-input reduced frequency and amplitude. After two or three cycles of motion, the airfoil was released and was allowed to follow the motion dictated by the structural dynamics equations. For the first case considered here, the structural parameters used were: $I = 37.5094$, $K_\alpha = 0.4054$, $g_\alpha = 6 \sim 9$. This case was chosen because it has been studied in a similar work by Ballhaus and Goorjian.[4]

In Fig. 6, the time histories associated with the lift, drag, and angle of attack α computed by the present approach at 0.9 Mach number are shown for the single-DOF flutter case. It is seen that a gradual variation in the structural damping coefficient g_α from 9.0 to 6.3 leads to a variation in the airfoil structural response ranging from damped oscillations to flutter solutions. It may be noted that Ballhaus and Goorjian[4] were the first to predict the single-DOF transonic flutter of the NACA 64A006 airfoil.

Next, a two-DOF flutter calculation is described. The airfoil chosen is a NACA 64A006 airfoil, with the pitch axis located at the quarter-chord. The freestream Mach number was 0.85 and the flow was assumed to be inviscid. This case has been previously studied by Guruswamy and Yang.[7] The airfoil was first subjected to a sinusoidal pitching oscillation at 0.01 rad amplitude at a reduced frequency of 0.05. The lift and pitching moment varitions are shown in Fig. 7 for the first few cycles of forced oscillations. (See Table 1 for a comparison between present results and Ref. 6.)

At the end of the third cycle of forced sinusoidal oscillations, the airfoil was released and was allowed to follow pitching and plunging motions dictated by the structural dynamics equations. The structural parameters used were: $\omega_h/\omega_\alpha = 0.2$, $a_h = -0.5$, $x_\alpha = 0.25$, $V^* = 5.5$, $k_\alpha = 0.05$, $\gamma_\alpha = 0.5$, $\mu = 150 \sim 200$, and have been used by Yang et al.[6] in a similar study. The airfoil-to-air-mass ratio was parametrically varied during this phase of the calculations to study the effects of the mass ratio on the flutter characteristics. As shown in Fig. 8, it was found that variations in the airfoil-to-air-mass ratio can lead to damped oscillations, neutral oscillations, or divergent (flutter) oscillations.

In Fig. 9, the flutter speed predicted by the present theory is plotted as a function of the airfoil-to-air-mass ratio for a set of structural parameters considered in Ref. 6. For comparison, the results from the LTRAN2 code[4] and the computer code UTRANS2[8] are shown. The UTRANS2 code solves the unsteady low- and high-frequency transonic small-disturbance equations in the frequency domain using a relaxation technique. It is seen that the Euler results agree very well with the predictions of the UTRANS2 code, while only a qualitative agreement between the present results and the LTRAN2 code could be found.

In order to assess the effects of flow viscosity on the flutter characteristics, these two-DOF flutter calculations were repeated, using the present flow solver operating in the Navier-Stokes mode. The structural parameters were same as those used for calculation shown on Fig. 8. The flow Reynolds number was set to 9×10^6. In Fig. 10, the time response, airfoil

Table 1 Comparison between present solution and Ref. 6 for case shown in Fig. 7[a]

Approach	$\lvert C_{L\alpha}\rvert$	Phase, deg	$\lvert C_{M\alpha}\rvert$	Phase, deg
Present	11.111	−37.6	0.608	−178.9
Ref. 6	12.319	−30.0	0.683	−171.0

[a] $|C_{L\alpha}|$ = normalized lift coefficient and $|C_{M\alpha}|$ = normalized moment coefficient.

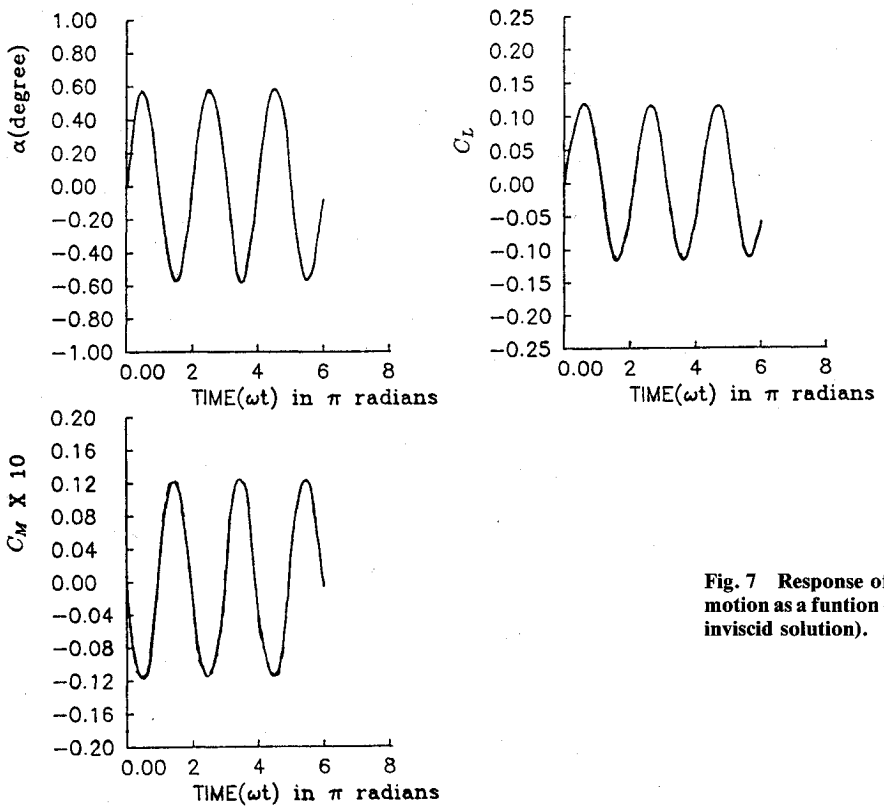

Fig. 7 Response of a NACA 64A006 airfoil to a sinusoidal pitching motion as a funtion of time ($M_\infty = 0.85$, $k_b = 0.05$, 0.01 rad amplitude, inviscid solution).

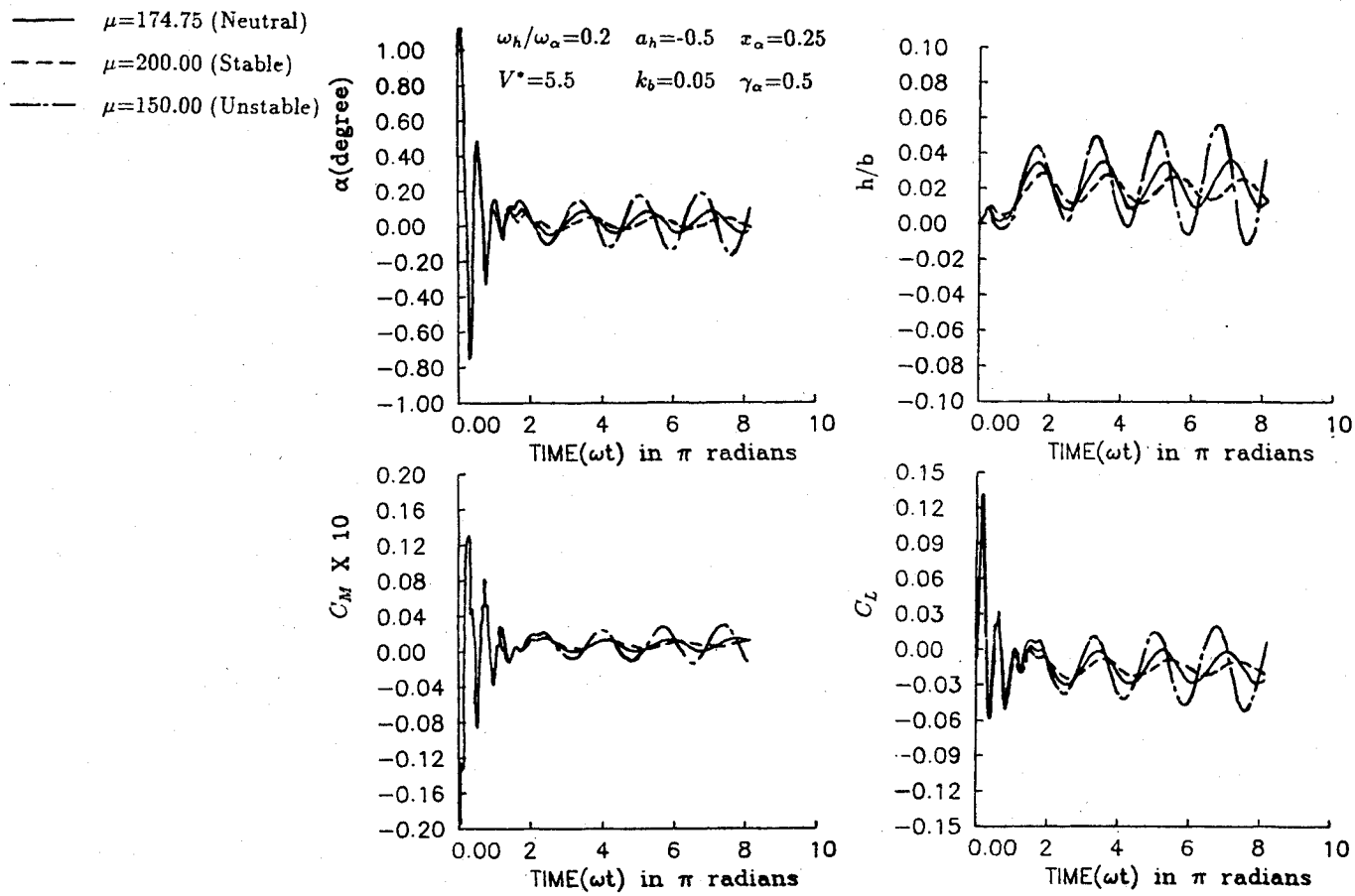

Fig. 8 Response of the solid-fluid system as a function of time (NACA 64A006 airfoil, $M_\infty = 0.85$, two-degree-of-freedom inviscid solution).

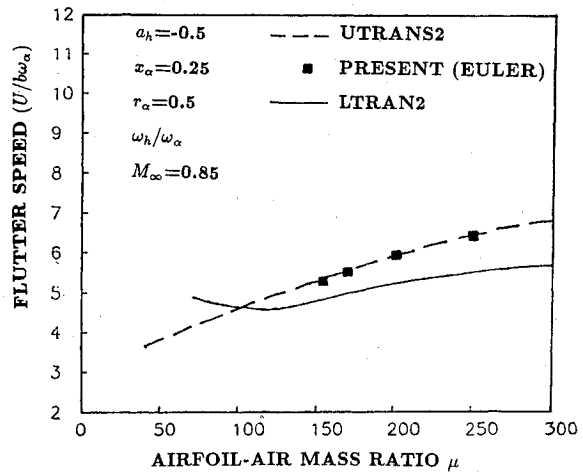

Fig. 9 Effect of airfoil air-mass ratio on the flutter speed of a two-degree-of-freedom solid-fluid system (NACA 64A006 airfoil, $M_\infty = 0.85$, inviscid solution).

angle of attack, lift, and moment are shown for the neutrally stable condition. This corresponds to a mass ratio of 170, which is slightly lower than the mass ratio values (174.75) predicted by the same solver operating in the inviscid mode. The shock strength and location are somewhat sensitive to the presence of the boundary layer on the airfoil surface and the viscous calculation showed consistently higher amplitude response than the inviscid calculations. Nevertheless, the flutter boundaries predicted by the viscous and the inviscid calculations were within 2% of each other, reinforcing the belief that, in high Reynolds number transonic flutter studies, inviscid calculations would suffice.

Stall Flutter Calculations

Two sets of stall flutter calculations were carried out using the Navier-Stokes/structural dynamics solver documented above. In the first case, the starting point was the steady viscous flow over a NACA 0012 airfoil at 0.3 Mach number and 9×10^6 Reynolds number at 15 deg angle of attack. At this angle of attack, the airfoil is on the verge of stall. The airfoil was given a small-amplitude perturbation in its angle of attack and the subsequent motion was studied in detail. The dimensionless speed V^* was varied between 4 and 8, while the structural parameters were the same as for Fig. 8. The airfoil response to these two dimensionless speed values are shown in Fig. 11. The other structural parameters used are also shown in this figure. It was found that at $V^* = 4$, the airfoil returned to steady state following a period of damped oscillations. For the higher dimensionless speed case, the airfoil oscillations grew rapidly with time and stall flutter was triggered, as clearly seen in Fig. 11.

The calculations shown above were repeated at lower angles of attack (8–10 deg), but no flutter solutions could be found. Thus, it appears that the flutter phenomenon observed in Fig. 11 is not a conventional flutter phenomenon, but is triggered by the stalled flow over the airfoil at higher angles of attack.

The second case considered also involved a NACA 0012 airfoil, initially subjected to a sinusoidal pitching oscillation between 5 and 25 deg. The freestream Mach number and Reynolds number were 0.283 and 3.45×10^6, respectively. During the downstroke, around 23.8 deg, the airfoil was released and was allowed to follow a pitching and plunging motion dictated by the structural dynamics equations. Two dimensionless speeds, $V^* = 4$ and 8, were considered. Again, at the lower speed the airfoil began to undergo a damped sinusoidal oscillation until it reached a force-free condition at zero degree angle of attack, as shown in Fig. 12. The time

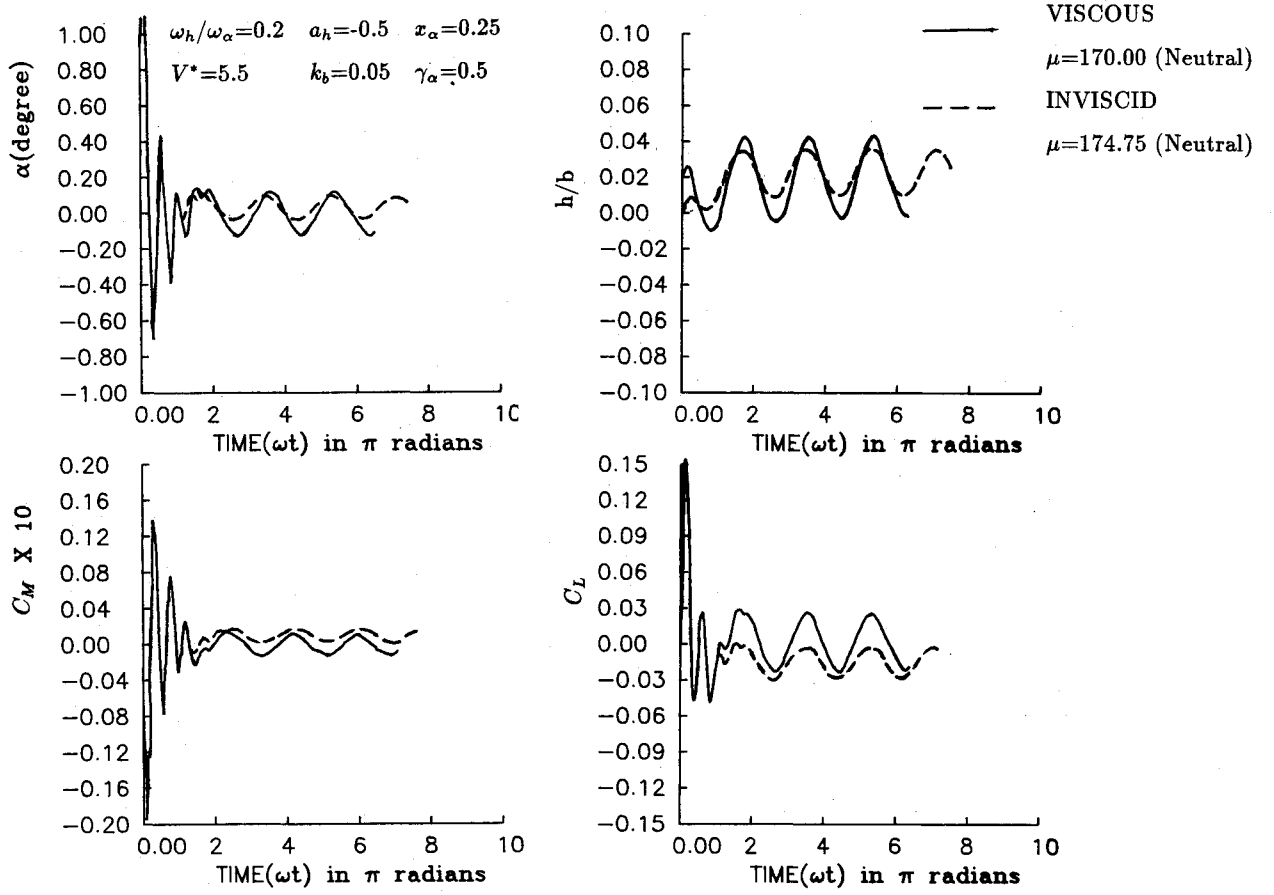

Fig. 10 Effect of viscosity on the time response of a solid-fluid system with two degrees of freedom (NACA 64A006 airfoil, $M_\infty = 0.85$, viscous solution corresponds to $Re = 9 \times 10^6$).

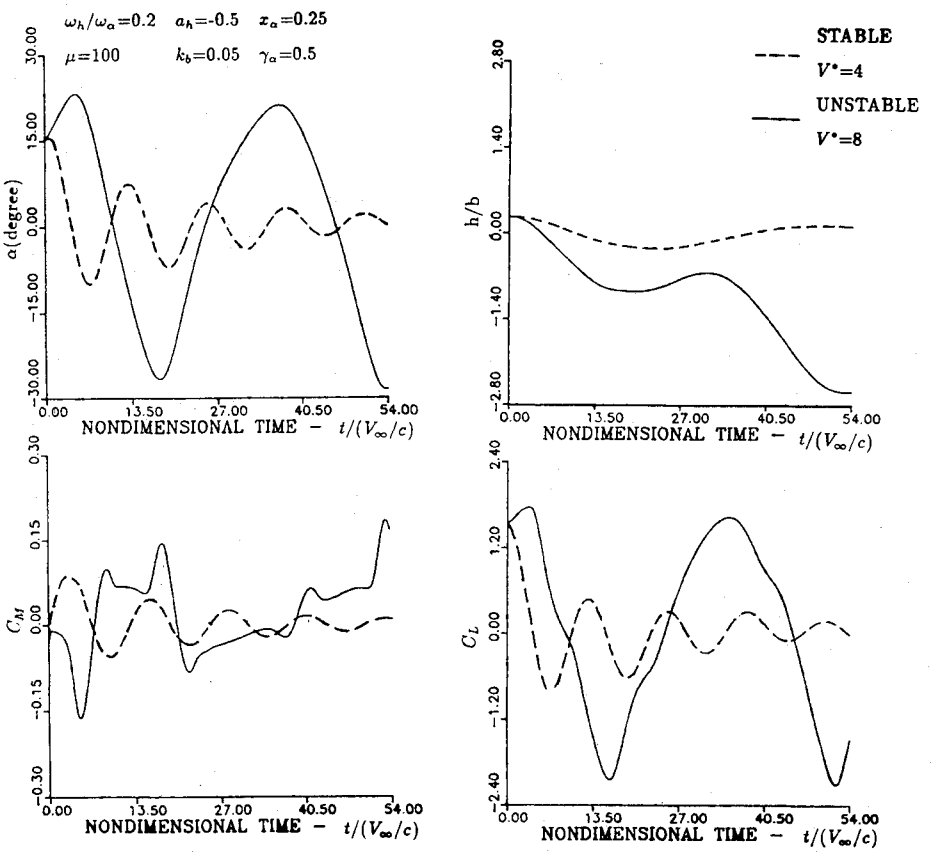

Fig. 11 Time response of a two-degree-of-freedom solid-fluid system experiencing stall flutter (NACA 0012 airfoil, $M_\infty = 0.3$, $Re = 9 \times 10^6$, initial angle of attack 15 deg).

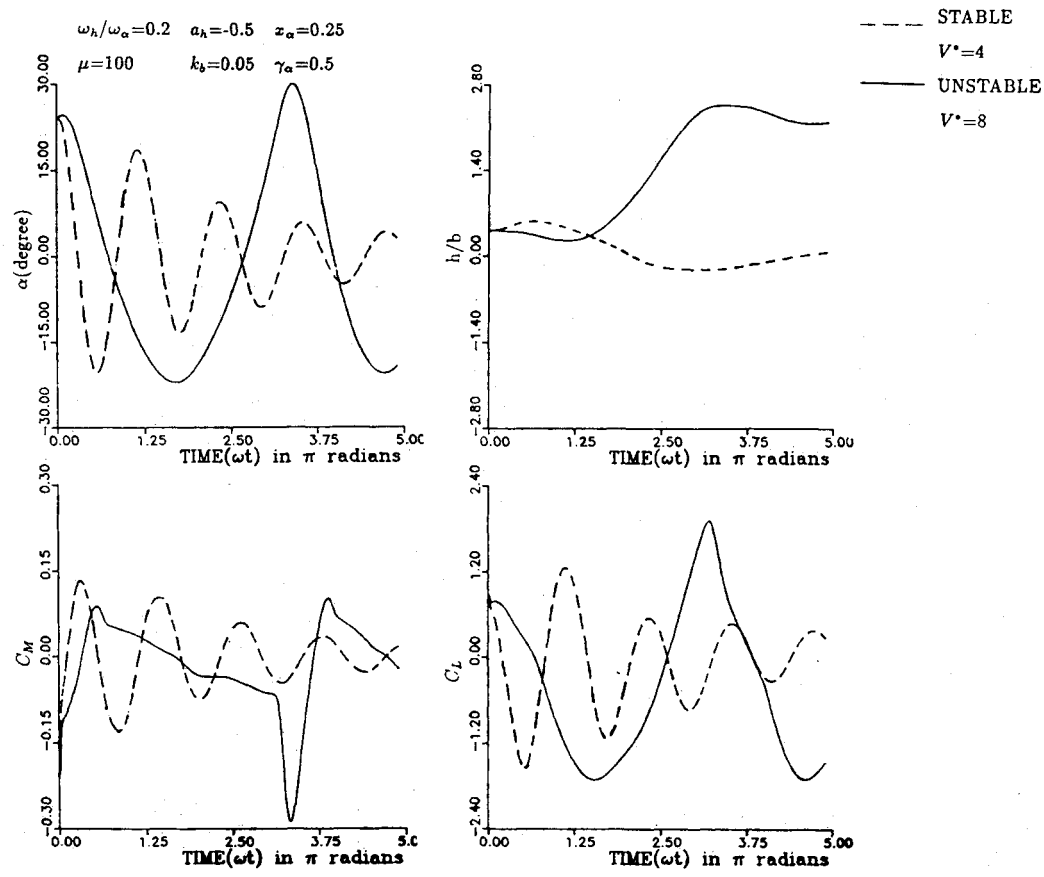

Fig. 12 Time response of a two-degree-of-freedom solid-fluid system experiencing stall flutter (NACA 0012 airfoil, $M_\infty = 0.283$, $Re = 3.45 \times 10^6$, initial angle of attack 23.82 deg).

history for the speed $V^* = 8$, however, showed a rapidly growing oscillatory motion indicative of stall flutter.

In these cases (Figs. 11 and 12), the damped and the stall flutter motions occurred at frequencies that roughly correspond to the natural frequency associated with the pitching motion. This leads to the conjecture the pitching mode is the most dominant mode in the stall flutter phenomena considered here.

Conclusions

A solution procedure has been developed for determining the transonic and subsonic flutter characteristics of airfoils at large mean angles of attack. For the transonic flutter calculations, this theory leads to flutter boundaries that are in agreement with the existing potential flow theories. In flutter calculations dominated by a single degree of freedom, the present calculations predict flutter onset at freestream Mach numbers above those predicted by the transonic potential flow theory.

Encouraging preliminary results have also been obtained for predicting the stall flutter. The stall flutter calculations reported here should be repeated using different turbulence models and on finer grids to assess what effects these factors play in the numerical prediction of this complex phenomenon.

Finally, good quality experimental data for one- and two-degree-of-freedom stall flutter are needed to validate this solver and similar solvers under development elsewhere.

Acknowledgments

This work was supported by the NASA Lewis Research Center under Grant NAG-3-730. This paper is dedicated to the memory of Dr. K. R. V. Kaza who passed away on July 26, 1988.

References

[1]Beddoes, T. S., "A Synthesis of Unsteady Aerodynamic Stall Hysteresis," *Proceedings of the First European Rotorcraft Forum,* 1975; also, *Vertica,* Vol. 1, No. 2, 1976.

[2]Gangwani, S. T., "Synthesized Airfoil Data Method for Prediction of Dynamic Stall and Unsteady Airloads," *Proceedings of the 39th Annual Forum of the AHS,* American Helicopter Society, Washington, DC, 1983.

[3]Reddy, T. S. R. and Kaza, K. R. V., "A Comparative Study of Some Dynamic Stall Models," NASA TM 88917, Dec. 1986.

[4]Ballhaus, W. F. and Goorjian, P.M., "Computation of Unsteady Transonic Flow by the Indicial Method," *AIAA Journal,* Vol. 16, Feb. 1978, pp. 117–126.

[5]Yang, T. Y., Stritz, A. G., Guruswamy, P., and Olsen, J. J., "Flutter Analysis of a NACA 64A006 Airfoil in Small Disturbance Transonic Flow," *Journal of Aircraft,* Vol. 17, April 1980, pp. 225–232.

[6]Yang, T. Y., Guruswamy, P. M., and Stritz, A. G., "Application of Transonic Codes to Flutter Analysis of Conventional and Supercritical Airfoils," *Journal of Aircraft,* Vol. 19, March 1982, pp. 211–220.

[7]Guruswamy, P. M. and Yang, T. Y., "Transonic Time Response Analysis of Thin Airfoils by Transonic Code LTRAN2," *Computers and Fluids,* Vol. 9, No. 4, 1981, pp. 409–425.

[8]Farr, J. L., Traci, R. M., and Albano, E. D., "Computer Programs for Calculating Small Disturbance Transonic Flows About Oscillating Airfoils," AFFDL-TR-74-135, Nov. 1974.

[9]Isogai, K., "Numerical Study of Transonic Flutter of a Two-Dimensional Airfoil," National Aerospace Lab., Japan, Rept. TR-617T, July 1980.

[10]Sankar, L. N. and Tassa, Y., "An Algorithm for Unsteady Transonic Flow Past Airfoils," *Proceedings of the Seventh International Conference on Numerical Methods in Fluid Dynamics,* June 1980.

[11]Eastep, F. E. and Olsen, J. J., "Transonic Flutter Analysis of a Rectangular Wing with Conventional Airfoil Sections," *AIAA Journal,* Vol. 18, Oct. 1980, pp. 1159–1164.

[12]Borland, C. J., Rizzetta, D. P., and Yoshihara, H., "Numerical Solution of Three-Dimensional Unsteady Transonic Flow Over Swept Wings," *AIAA Journal,* Vol. 20, March 1982, pp. 340–347.

[13]Borland, C. J. and Rizzetta, D. P., "Non-Linear Transonic Flutter Analysis," *AIAA Journal,* Vol. 20, Nov. 1982, pp. 1606–1615.

[14]Sankar, L. N., Malone, J. B., and Tassa, Y., "An Implicit Conservative Algorithm for Steady and Unsteady Three-Dimensional Transonic Potential Flows," *Proceedings of the 5th Computational Fluid Dynamics Conference,* June 1981.

[15]Edwards, J. W. and Thomas, J. L., "Computational Methods for Unsteady Transonic Flows," AIAA Paper 87-0107, Jan. 1987.

[16]Steger, J. L. and Bailey, H. E., "Computation of Transonic Aileron Buzz," *AIAA Journal,* Vol. 18, 1980, pp. 249–255.

[17]Wu, J.-C., "A Study of Unsteady Turbulent Flow Past Airfoils," Ph.D. Dissertation, Georgia Inst. of Technology, Atlanta, GA, Aug. 1988.

[18]Sorenson, R. L., "A Computer Program to Generate Two-Dimensional Grids About Airfoils and Other Shapes by the Use of Poisson's Equation," NASA TM 81198, May 1980.

[19]Beam, R. M. and Warming, R. F., "An Implicit Factored Scheme for the Compressible Navier-Stokes Equations," *AIAA Journal,* Vol. 16, April 1976.

[20]Steger, J. L., "Implicit Finite Difference Simulation of Flow About Arbitrary Two-Dimensional Geometries," *AIAA Journal,* Vol. 18, July 1978, pp. 679–686.

[21]Baldwin, B. S. and Lomax, H., "Thin Layer Approximation and Algebraic Model for Separated Turbulent Flows," AIAA Paper 78-0257, 1978.

[22]McAlister, K. W., Pucci, S. L., McCroskey, W. J., and Carr, L. W., "An Experimental Study of Dynamic Stall in Advanced Airfoil Sections, Vol. 2, Pressure and Force Data," NASA TM 84245, Sept. 1982.